

## Competition between delocalization and spin-orbit splitting in the actinide $5f$ states

J. G. Tobin,<sup>1,\*</sup> K. T. Moore,<sup>1</sup> B. W. Chung,<sup>1</sup> M. A. Wall,<sup>1</sup> A. J. Schwartz,<sup>1</sup> G. van der Laan,<sup>2</sup> and A. L. Kutepov<sup>3</sup>

<sup>1</sup>Lawrence Livermore National Laboratory, Livermore, California 94550, USA

<sup>2</sup>Synchrotron Radiation Source, Daresbury Laboratory, Warrington, WA4 4AD, United Kingdom

<sup>3</sup>Russian Federation Nuclear Center, Institute of Technical Physics (VNIITF), Snezhinsk, Chelabinsk Region, Russia

(Received 27 October 2004; revised manuscript received 17 February 2005; published 4 August 2005)

Synchrotron-radiation-based x-ray absorption, electron energy-loss spectroscopy in a transmission electron microscope, multielectronic atomic spectral simulations, and improved first-principles calculations (generalized gradient approximation in the local density approximation) have been used to investigate the electronic structure of the light actinides:  $\alpha$ -Th,  $\alpha$ -U, and  $\alpha$ -Pu. It will be shown that the spin-orbit interaction can be used as a measure of the degree of localization of valence electrons in a material. The spin-orbit interaction in the light actinide metals  $\alpha$ -Th,  $\alpha$ -U, and  $\alpha$ -Pu, has been determined using the branching ratio of the white line peaks of the  $N_{4,5}$  edges, which correspond to  $4d \rightarrow 5f$  transitions. Examination of the branching ratios and spin-orbit interaction shows that the apparent spin-orbit splitting is partially quenched in  $\alpha$ -U, but is strongly dominant in  $\alpha$ -Pu. These results are fully quantified using the sum rule. This picture of the actinide  $5f$  electronic structure is confirmed by comparison with the results of electronic structure calculations for  $\alpha$ -Th,  $\alpha$ -U, and  $\alpha$ -Pu, which in turn are supported by a previous bremsstrahlung isochromat spectroscopy experiment.

DOI: [10.1103/PhysRevB.72.085109](https://doi.org/10.1103/PhysRevB.72.085109)

PACS number(s): 71.10.-w, 71.20.Gj, 71.27.+a, 71.28.+d

### I. INTRODUCTION

Understanding the behavior of  $5f$  electrons remains an important and unachieved goal of condensed-matter physics. Recently, there has been a surge of interest in the actinides, particularly plutonium, driven by the variety of exotic behaviors exhibited by these systems, prompting both theoretical and experimental investigations of  $5f$  metals and compounds.<sup>1-10</sup> Intriguingly, investigations of these exotic behaviors, such as the profoundly large increase in atomic volume that occurs at plutonium,<sup>9,10</sup> or the discovery of Pu-based superconductivity,<sup>6-8</sup> or observation of previously unmeasured quantities such as the phonon dispersion in Pu,<sup>3-5</sup> all point back to the  $5f$  electronic structure as the cause or origin of the anomalies and strange behavior. However, to unravel the enigma of actinide electronic structure, it is necessary to quantify the central event within the actinide series, the localized-itinerant transition of the  $5f$  electrons. The  $5f$  electrons behave in a localized or correlated fashion for the heavy actinides but in a more delocalized manner for the light actinides, with a nexus in the vicinity of Pu and Am. There has yet to be a quantitative and definitive determination of this phenomenon, leaving it as an unanswered question of actinide condensed-matter physics. Resolving this question will facilitate both a wider understanding of the exotic behaviors of the actinides and a significant refinement of the theoretical framework of computational models of the actinides.

To quantify the competition between spin-orbit splitting and delocalization, our experimental and simulated spectra will be analyzed in terms of what is called a branching ratio and spin-orbit interaction.<sup>11-13</sup> By comparing experimental results with spectral simulations arising from three different types of atomic models, the spin-orbit interaction can be used as a local probe for the competition between spin-orbit splitting and delocalization in the valence band of a material. Transition metals, rare earths, and actinides exhibit high-intensity peaks at the threshold of absorption edges called

white lines, that are due to electric dipole transitions from core states to the empty states of the valence band. The branching ratio of the white lines is directly related to the expectation value for the spin-orbit operator in the valence states. Using multielectronic, atomic spectral simulations, which include angular momentum coupling and Coulomb and exchange interactions, it is possible to predict the responses of a core-level spectrum within various coupling schemes. By comparing experimental results with the predictions of the multielectronic atomic models, a measure of the degree of localization of the valence electrons can be established. In the actinides, this can be pursued using either the  $3d$  or  $4d$  initial state,<sup>13</sup> but not the  $5d$ , as the spin-orbit separation in the  $5d$  manifold is too small, in the order of 10 eV.<sup>14</sup> In the case of the  $4d$  initial state, the spin-orbit splitting is on the scale of 40–50 eV and the white line for each  $4d \rightarrow 5f$  transition is clearly resolved, making the  $N_{4,5}$  edge suitable for branching ratio determination.

It is the focus of this paper to quantitatively determine the relative impact of the spin-orbit splitting and delocalization in the actinide  $5f$  states, using the degree of spin-orbit interaction in the  $5f$  states of the light actinides via the branching ratio of the white lines present in the  $N_{4,5}(4d \rightarrow 5f)$  transition and state-of-the-art calculations of the valence band density of states. The spectral analysis will be achieved using electron energy-loss spectroscopy (EELS) in a transmission electron microscope (TEM), synchrotron-radiation-based x-ray absorption (XAS), and multielectronic atomic spectral simulations. These results will then be discussed within the context of the projected density of states of these actinides, including generalized gradient approximation (GGA) local density approximation (LDA) calculations of the electronic structure of  $\alpha$ -Th,  $\alpha$ -U, and  $\alpha$ -Pu, which include a more exact treatment of spin-orbit splitting in the  $5f$  states.

### II. EXPERIMENTAL AND COMPUTATIONAL DETAILS

EELS experiments were performed using a Phillips CM300 field-emission-gun TEM, equipped with a Gatan im-

aging filter for the collection of spectra. Since the accelerating voltage of the TEM was 300 keV and much larger than the energy of the  $N_{4,5}$  transitions for Th, U, and Pu, the electron transitions are justified as electric dipole.<sup>15</sup> (This assertion will be experimentally verified via direct comparison with the corresponding x-ray absorption spectra.) EELS spectra were recorded in imaging mode using a collection angle of 6 mrad, which allowed the 000 beam and the first-order reflections to contribute to the spectra. All spectra were reproduced numerous times using a sample thickness of approximately 0.5 inelastic mean free paths, as calculated by the zero-loss and plasmon peaks. Background removal was performed using a log-polynomial extrapolation and various window placements to ensure correct and consistent background extrapolation. Multiple spectra were recorded, aligned, and summed to optimize the signal-to-noise ratio and to maintain optimal energy resolution of about 1 eV. Samples were 99.9% pure and were prepared via either electropolishing or ion milling. While Th and U could be handled directly, all Pu work was performed in a glove box, and the samples were transported in a vacuum-transfer holder due to the toxic nature of the metal. The full procedure for Pu sample preparation is described by Wall *et al.*<sup>16</sup> and Moore *et al.*<sup>17</sup> There was a small amount of oxide on the surface of the TEM samples, but it was negligible in comparison to the approximately 50 nm of metal sampled through transmission of the electron beam. The XAS spectra were collected in total-yield mode, using a 30 mg sample of purified  $\alpha$ -Pu, at the Advanced Light Source. The details are provided elsewhere.<sup>18,19</sup> Needless to say, the experiments with Pu were hampered by its high level of radioactivity and chemical toxicity, and strong tendency to react.

We will show here results of two different types of calculations, namely, (1) atomic calculations to obtain ground-state properties and their excitation spectra and (2) density functional calculations for the density of states in the ground state. The atomic spectral simulations are based upon earlier work by Thole and van der Laan.<sup>11–13,19</sup> While the underlying single-electron physics is the same in each of the three models, the differences arise when electrons are allowed to interact or “tangle.” The impact of this will be described below.

An improved version of density functional theory (DFT) in the generalized gradient approximation<sup>20</sup> has been used in the present work to study the electronic and magnetic structure for thorium, uranium, and plutonium. Importantly, all calculations were performed with the full-potential, Dirac relativistic ( $j, m_j$ )-basis, spin-polarized (collinear with the  $Z$  axis as an axis of quantization) linearized-augmented-plane-wave method<sup>21</sup> (RSPFLAPW) and the real crystal structures were used:  $\alpha$ -Pu is monoclinic,  $\alpha$ -uranium is orthorhombic, and  $\alpha$ -thorium is fcc. As a result of this exact treatment, spin-orbit splitting in the  $5f$  states is treated in a more fundamental manner and knowledge of the  $j$ -state parentage of the states within the  $5f$  density of states DOS is retained. As will be shown below, this retention of parentage information is of great importance. The calculational parameters such as the number of  $\mathbf{k}$  points, size of the basis set, and others, were chosen in such a manner that the convergence of the total energy was better than 1 mRy/atom. 30 irreducible  $\mathbf{k}$  points

have been used for  $\alpha$ -Pu, 105 for  $\alpha$ -U, and 195 for  $\alpha$ -Th. The size of the basis set was about 450 functions/atom for  $\alpha$ -Pu, and about 200 functions/atom for  $\alpha$ -U and  $\alpha$ -Th. Results for the eight different sites in  $\alpha$ -Pu are shown in Fig. 1, including two different cases: nonmagnetic (NM) and antiferromagnetically (AF) aligned Pu. While it is well known that there is no experimental evidence for the existence of a magnetic moment in Pu, significant physical insights can be gleaned from such computational simulations. Moreover, in Ref. 21 the following was pointed out. “There are many configurations (generally speaking with magnetic order) in the electronic system of  $\alpha$ -Pu, which have almost equal energies. These configurations are characterized by different directions of magnetic moments in the atoms. When the temperature increases (above absolute zero), the system fluctuates between them in such a manner that the magnetic moments of the atoms are equal to zero on average.” Thus, even in the “magnetic” model of  $\alpha$ -Pu, the net moment on each Pu atom is zero. This subject will be discussed in more detail below.

### III. DISCUSSION

The  $N_{4,5}(4d \rightarrow 5f)$  white line spectra (XAS, EELS, and spectral simulation) are shown in Fig. 2 for  $\alpha$ -Pu.<sup>19</sup> For comparison, the  $M_{4,5}(3d \rightarrow 4f)$  white line spectra (XAS, EELS, and spectral simulations) for Ce are also included. Accompanying each set is the single-crystal diffraction pattern taken in the TEM in concert with the EELS measurements, directly confirming the phase of each sample. The spin-orbit-split initial states ( $4d_{5/2}$  and  $4d_{3/2}$  in Pu and  $3d_{5/2}$  and  $3d_{3/2}$  in Ce) are clearly resolved for each metal as a pair of white lines. While the Ce exhibits a significant fine structure, none is resolved for either edge in Pu because the intrinsic lifetime broadening is about 2 eV for both core levels in Pu.<sup>14,22</sup> Along the actinide series from Th to Pu the  $4d_{3/2}$  peak progressively reduces in intensity relative to the  $4d_{5/2}$  peak due to the fact that selection rules require that a  $d_{3/2}$  core-level electron can only be excited into an  $f_{5/2}$  level.<sup>13,19</sup> Because of the low  $4f$  occupation in Ce, such a strong relative reduction in the  $d_{3/2}$  peak intensity is not observed in Ce. (However, a similar but weaker trend is also observed for rare earths, where the ground state is still far enough from  $LS$  coupling to give a significant effect. This trend in the peak ratio is very clearly visible in Fig. 1 of Ref. 23. In the case of Ce compounds, the trend in the branching ratio has been used to obtain the relative population of the spin-orbit split states.<sup>24</sup>) Thus the decrease in intensity of the Pu  $4d_{3/2}$  peak in Fig. 2 illustrates a progressive filling of the  $5f_{5/2}$  level along the actinide series, as previously observed.<sup>19,25</sup> While our  $\alpha$ -Pu EELS spectrum is self-confirmed by our  $\alpha$ -Pu XAS spectrum, our  $\alpha$ -U EELS spectrum (not shown; see Ref. 19) can be confirmed by comparison to the  $\alpha$ -U XAS spectrum in Fig. 3 of Ref. 22. In fact, the small features observed in the background of the EELS spectra, between the much larger  $4d_{3/2}$  and  $4d_{5/2}$  peaks, are similar to those reported in Ref. 22.

We may now use the areas beneath the  $N_4(4d_{3/2} \rightarrow 5f)$  and the  $N_5(4d_{5/2} \rightarrow 5f)$  white line peaks to calculate the

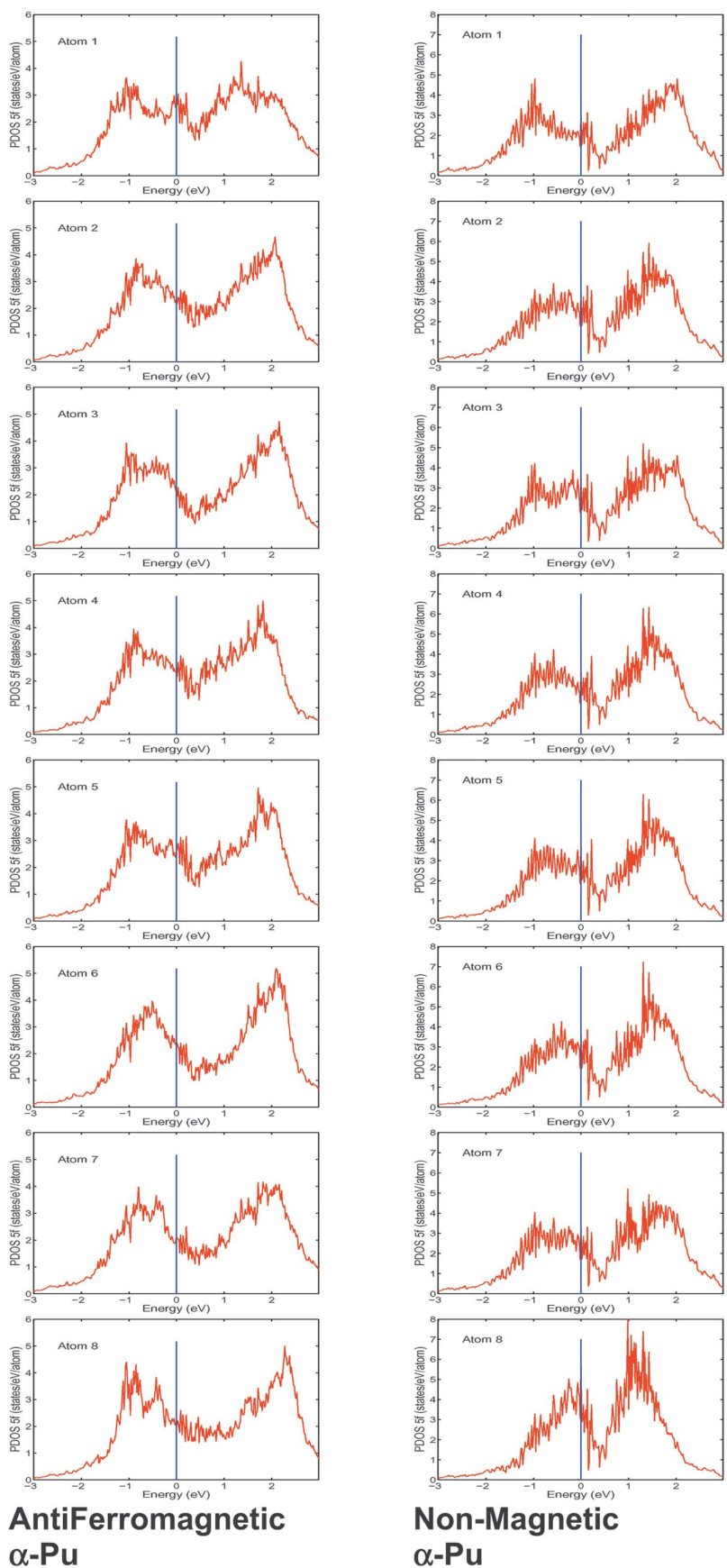


FIG. 1. (Color) Calculations of the density of states for  $\alpha$ -Pu are shown here, as described in the text. States below the Fermi level (negative energies) are occupied and states above the Fermi level (positive energies) are unoccupied. The Fermi level is at 0 eV. See Ref. 21.

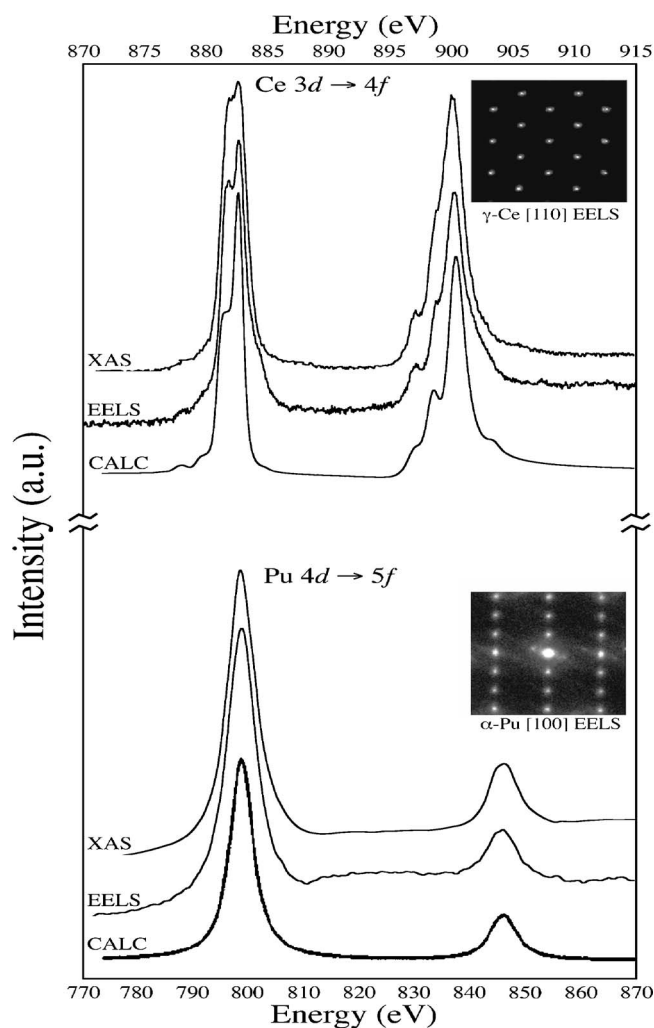


FIG. 2. White line spectra  $\alpha$ -Pu ( $N_{4,5}, 4d \rightarrow 5f$ ) and Ce ( $M_{4,5}, 3d \rightarrow 4f$ ) acquired by EELS in a TEM, XAS, and spectral simulation are shown here. A single-crystal diffraction pattern from each metal is presented, confirming the phase being examined by EELS. For Ce, the  $3d_{5/2}$  peak is near 884 eV and the  $3d_{3/2}$  peak is near 902 eV. For Pu, the  $4d_{5/2}$  peak is near 798 eV and the  $4d_{3/2}$  peak is near 845 eV (Ref. 14). Note the significantly different energy scales for Ce and Pu.

branching ratio ( $B$ ), which is summarized in Table I and plotted in Fig. 3 as a function of the number of  $5f$  electrons ( $n$ ). Here we have used  $n=0.6$  for Th,<sup>26</sup> 3 for U,<sup>27</sup> and 5 for Pu.<sup>27</sup>

Before going on to a consideration of the branching ratios versus  $5f$  occupation number, a brief digression on  $5f$  occupancy is appropriate. In general, determining the number of  $5f$  electrons in an actinide atom or ion is an involved and often controversial process. In the case of uranium compounds and intermetallics, the effect of varying oxidation state can easily be seen in the spectra in Fig. 2 of Kalkowski *et al.*<sup>22</sup> For U compounds, covalency<sup>28</sup> and transfer interactions with the  $6d$  levels<sup>29</sup> remain subjects of discussion. However, in this study we are primarily concerned with “pure” or elemental actinides: Th, U, and Pu. In the case of Th, we have used  $n=0.6$ . This number is close to the value of  $n=1/2$  proposed by Baer and Lang,<sup>26</sup> based upon their inter-

pretation of the work of Skriver and Jan.<sup>30</sup> However, given the Th experimental branching ratio, our calculations reveal that there must be a  $5f$  occupation of 0.6 or greater in order to have a non-negative  $5f_{7/2}$  occupation. Thus, we have used  $n=0.6$  for Th in this work. For Pu, the situation is even more clear-cut. A value of  $n=5$  is consistent with a number of theoretical works (Ref. 25 and references therein, and Ref. 31) and is strongly supported by the analysis of our x-ray absorption and electron energy loss spectra for a lower-lying transition ( $5d \rightarrow 5f$ ) in Pu, as described elsewhere.<sup>25</sup> The value of  $n=5$  for Pu also is consistent with the consensus viewpoint expressed in the spectral review by Naegele.<sup>27</sup> Thus, for Pu, there is strong evidence for  $n=5$ . Finally, let us consider the controversial case of elemental U. At one point it was proposed that  $n=0$  for U, but in 1980 it was demonstrated by Johansson *et al.*<sup>32</sup> that  $n>0$  for U. Around the same time, a number of works came out in favor of  $n>2$  for U.<sup>26,31,33,34</sup> In the more recent past, there seems to be something of a consensus that  $n=3$  approximately for U, as illustrated in the works of Zangwill and Liberman<sup>35</sup> and Laubschat, Grentz, and Kaindl<sup>36</sup> as well as the spectral review by Naegele.<sup>27</sup> Nevertheless, in recognition of the past controversies, we have put horizontal error bars of  $\pm 1/2$  on all experimental data points in both Figs. 3 and 4(a).

Figure 3 contains the branching ratios for the EELS spectra of  $\alpha$ -Th,  $\alpha$ -U, and  $\alpha$ -Pu,<sup>19</sup> and the  $\alpha$ -Pu XAS spectrum,<sup>18,19</sup> as well as that for  $\alpha$ -U XAS from Kalkowski *et al.*<sup>22</sup> For comparison, branching ratios derived from the simulated spectra shown in Fig. 2 of Ref. 13 are also included. These results are from an atomic, multielectronic model. The branching ratio for the  $4d \rightarrow 5f$  transition of the actinides is defined as

$$B = A_{5/2} / (A_{5/2} + A_{3/2}), \quad (1)$$

where  $A_{5/2}$  and  $A_{3/2}$  are the integrated intensities of the  $4d_{5/2}$  and  $4d_{3/2}$  peaks, respectively. Examination of Fig. 3 shows that the calculated branching ratios for  $n=0-5$  exhibit a roughly linear dependence. The experimental branching ratios for Th and Pu are near this line with their error bars intersecting the line, but the  $B$  of uranium falls well below it, even including the error bars. The branching ratio of U lies closer to the ideal statistical value of  $B_0=3/5$ : it will be shown below that this means that the U  $5f$  states are more itinerant and that the apparent spin-orbit splitting is partially quenched. On the other hand, Pu lies at a value of  $B$  more consistent with the strong spin-orbit interaction of the intermediate coupling model of the  $5f$  states, confirming a departure from an  $LS$  coupling behavior.<sup>19,25</sup> It will also be shown that while the  $B$  value of Th agrees nicely with the intermediate coupling model prediction, the  $5f$  occupation of Th is small enough that either  $LS$ ,  $jj$ , or intermediate coupling will accurately describe the state. In order to demonstrate the validity of these assertions, it is necessary to consider the branching ratios more analytically.

Within a sum rule model,<sup>11-13,19</sup> it is possible to express  $B$  as follows:

TABLE I. The values for the number of  $5f$  electrons ( $n$ ), the branching ratio ( $B$ ), the statistical value ( $B_0$ ), the spin-orbit operator  $\langle w^{110} \rangle$ , the number of  $5f$  electrons in the  $5/2$  level,  $n_{5/2}$ , and the number of  $5f$  electrons in the  $7/2$  level,  $n_{7/2}$ , used in Figs. 2 and 3. The XAS data are from Refs. 18 and 22.  $\langle w^{110} \rangle^C$  is the spin-orbit operator expectation value obtained using the calculated  $B_0$  from the intermediate coupling theory. The peak ratio for XAS U is reported on p. 2675 of Ref. 22.

	$n$	$B$	$\langle w^{110} \rangle$	$n_{5/2}$	$n_{7/2}$	$B_0$	$\langle w^{110} \rangle^C$
Calculations in intermediate coupling	0	0.592	0	0	0	0.592	
	1	0.634	-1.33	1	0	0.586	
	2	0.680	-2.57	1.96	0.04	0.594	
	3	0.723	-3.50	2.79	0.21	0.596	
	4	0.760	-4.04	3.45	0.55	0.598	
	5	0.817	-4.88	4.23	0.77	0.600	
Statistical distribution	$n$	$3/5$	0	$3n/7$	$4n/7$	$3/5$	
$jj$ coupling	$n \leq 6$	$3/5 + (8n/15nh)$	$-4n/3$	$n$	0	$3/5$	
Experiment							
EELS—Th	0.6 <sup>a</sup>	0.623	-0.77	0.59	0.01	0.589	-1.16
XAS—U (Kalkowski <i>et al.</i> )	3 <sup>b</sup>	0.676	-2.09	2.18	0.82	0.596	-2.20
EELS—U	3 <sup>b</sup>	0.685	-2.34	2.28	0.71	0.596	-2.45
XAS—Pu (Tobin <i>et al.</i> )	5 <sup>c</sup>	0.813	-4.79	4.20	0.80	0.600	-4.79
EELS—Pu	5 <sup>c</sup>	0.826	-5.09	4.32	0.67	0.600	-5.09

<sup>a</sup>Reference 26 reports a Th  $5f$  occupation of 0.5. However, given the Th experimental branching ratio, our calculations reveal that there must be a  $5f$  occupation of 0.6 or greater in order to have a non-negative  $5f_{7/2}$  occupation.

<sup>b</sup>Reference 27 p. 226:  $n_U = 3 - \varepsilon$ ; assume that  $\varepsilon \rightarrow 0$ , then  $n_U \rightarrow 3$ .

<sup>c</sup>Reference 27 p. 226:  $n_{Pu} = 5 - \xi$ ; assume that  $\xi \rightarrow 0$ , then  $n_{Pu} \rightarrow 5$ .

$$B = B_0 - (2/5)x. \quad (2)$$

$$x = \langle w^{110} \rangle / n_h = [n_h^{7/2} - (4/3)n_h^{5/2}] / (n_h^{7/2} + n_h^{5/2}). \quad (3)$$

$B_0$  is the statistical value, which equals  $3/5$  in the absence of core-valence interactions.  $x$  is proportional to the effective spin-orbit interaction per valence hole, or more precisely,

Here,  $n_h, n_h^{7/2}$ , and  $n_h^{5/2}$  are the number of holes in the  $5f$ ,  $5f^{7/2}$ , and  $5f^{5/2}$  levels, respectively. (Note that  $n_h = 14 - n$ ,  $n_h^{7/2} = 8 - n_{7/2}$ , and  $n_h^{5/2} = 6 - n_{5/2}$ , for comparison with Table I.)  $\langle w^{110} \rangle$  is the spin-orbit interaction expectation value.

The branching ratio depends on two parameters: the angular part of the valence spin-orbit interaction and the core-valence interaction.<sup>23,37</sup> If we neglect the core-valence interaction, then the branching ratio is a sum rule that is exact for all coupling schemes:  $LS$ ,  $jj$ , and intermediate. When the core-valence interactions are included, then  $B_0$  will be affected. For instance, in the  $3d$  and rare earth metals the application of the spin-orbit sum rule is hampered by a large core-valence interaction. However, in the case of the actinides the core-valence interactions in the  $N$ -edge and  $M$ -edge spectra are sufficiently small that the spin-orbit sum rule applies. Our calculations show that  $B_0$  varies between only 0.59 and 0.60 for the actinide  $N$  edge,<sup>19</sup> meaning that the EELS and XAS branching ratio is proportional almost solely to the expectation value of the spin-orbit interaction. (See Table I.)

We may now examine the issue of electron coupling more closely using the spin-orbit operator  $\langle w^{110} \rangle$ , which is a coupled tensor (one-particle operator) for the orbital and spin moments of the shell coupled to a total moment of order zero (scalar),<sup>13</sup> and it follows from Eqs. (2) and (3) that

$$\langle w^{110} \rangle = -\frac{5}{2}(B - B_0)n_h, \quad (4)$$

where  $n_h$  is the total number of holes in the  $5f$  state ( $n_h = 14 - n$ ). In Table I, the spin-orbit operator  $\langle w^{110} \rangle$  is shown

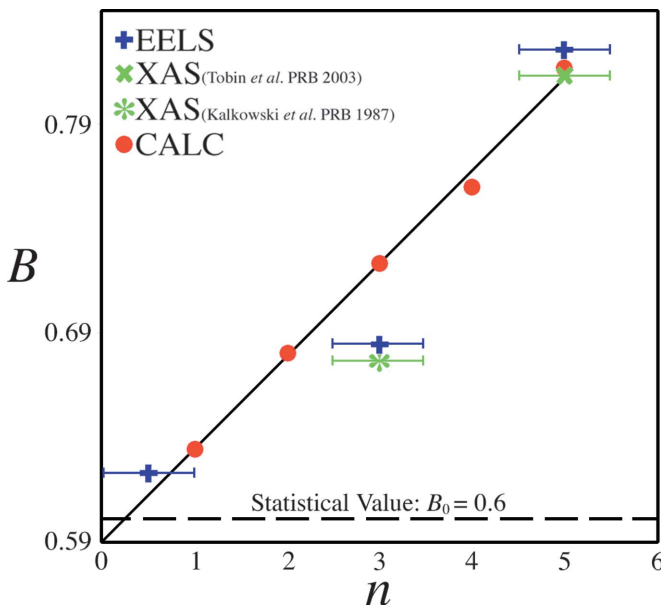


FIG. 3. (Color) The branching ratio ( $B$ ) as a function of the number of  $5f$  electrons ( $n$ ). The ideal statistical value of the branching ratio for the  $5f$  states ( $B_0$ ), which is  $3/5$  or 0.6, is shown along the bottom of the plot.

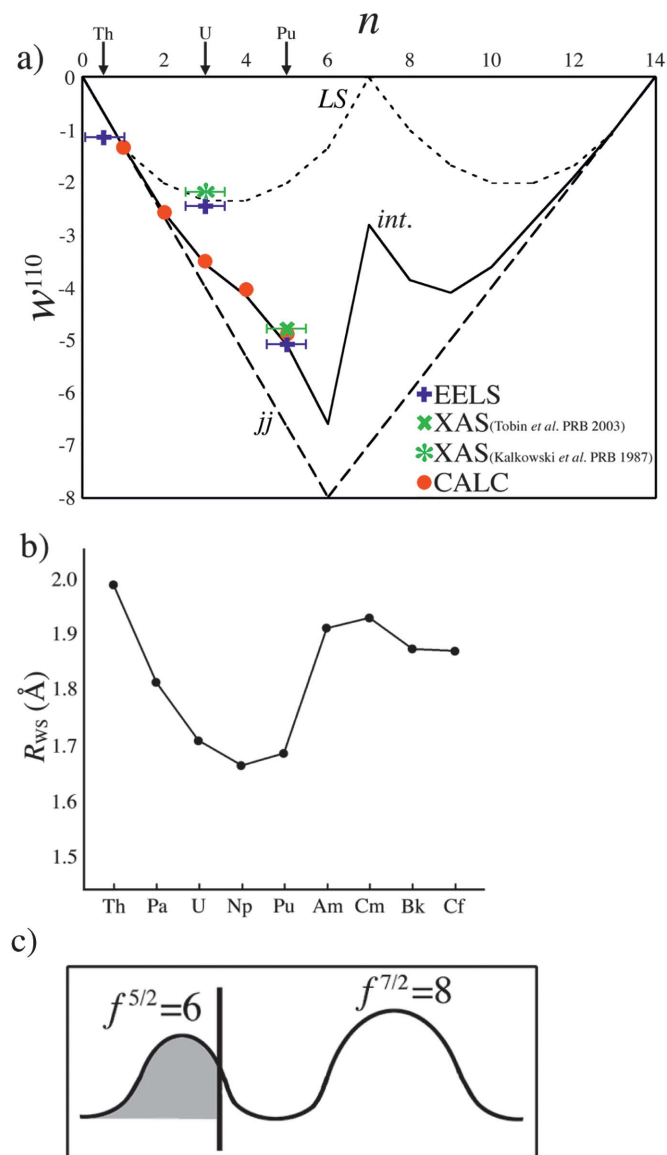


FIG. 4. (Color) (a) A plot of the expectation value of the spin-orbit operator  $\langle w^{110} \rangle$  as a function of the number of 5f electrons ( $n$ ). The three different electron coupling schemes are plotted;  $LS$  (short dash),  $jj$  (long dash), and intermediate coupling (solid). Notice how U falls directly on the  $LS$  curve, while Pu falls directly on the intermediate coupling curve. (b) A plot of the Wigner-Seitz atomic radius as a function of the actinide metal series (after Ref. 10). (c) Illustration of our simple model of the Pu 5f electronic DOS, with  $n=5$ . See text for details.

for the experimental and simulated data points. For the experimental values, the statistical value of  $B_0=3/5$  was used. In the case of the calculated values from the intermediate coupling model, the calculated  $B_0$  values (0.59–0.60) were utilized. Using the nonstatistical values of  $B_0$  with the experimental data caused only a negligible effect, as shown in Table I under  $\langle w^{110} \rangle^C$ , with the superscript  $C$  standing for “corrected.” The experimental and calculated  $\langle w^{110} \rangle$  values are plotted in Fig. 4(a), along with the results from Ref. 13 for three different electron coupling schemes:  $LS$  (short dash),  $jj$  (long dash), and intermediate coupling (solid). Notice that while the results for U are well approximated by an

$LS$  coupling scheme, Pu  $\langle w^{110} \rangle$  values are almost directly on the intermediate coupling curve. This explains why band calculations such as the simple local density approximation work well with U, but fail for Pu, as will be discussed further below.

Another way to address this question of angular momentum coupling is to look at the occupation of the  $5f_{5/2}$  and  $5f_{7/2}$  manifolds. However, it should be noted that this is not an independent proof but merely another way to view the problem. We can define a fractional occupation  $D$  as follows:

$$D = n_{7/2}/(n_{7/2} + n_{5/2}) = (4/7) + (3\langle w^{110} \rangle/7n), \quad (5)$$

with  $n_{7/2}$  and  $n_{5/2}$  obtained from Eq. (3):

$$n_{7/2} = (4/7)n + (3/7)\langle w^{110} \rangle, \quad (6)$$

$$n_{5/2} = n - n_{7/2}. \quad (7)$$

From this, we can trivially calculate  $n_{7/2}$  and  $n_{5/2}$ . The results are shown in Table I, as well as the predictions for the two limiting cases, the statistical value model and the  $jj$  coupling model. Again, the 5f occupation values of Th and Pu are consistent with the intermediate coupling model result, but the  $n_{7/2}$  and  $n_{5/2}$  values of U have substantially deviated from the predictions of the intermediate coupling case.

The enhanced population in the  $5f_{7/2}$  manifold and the reduced population in the  $5f_{5/2}$  manifold in U make sense. It has been demonstrated many times that the simpler LDA-type computational models work well to explain the photoemission spectra and other experimental results for uranium.<sup>26,27,38</sup> If a delocalization perturbation is overlaid upon a pair of spin-orbit-split manifolds of states, perturbation theory says that the previously separated states within each manifold may mix. In this case, states within each pure 5/2 and 7/2 manifold mix beyond the level associated with the intermediate coupling scheme, to a level comparable to an  $LS$  coupling scheme. Thus, although U is a delocalized-perturbed intermediate coupling scheme system, it accidentally looks like a Russell-Saunders ( $LS$ ) case, making it a good candidate for analysis with the simpler LDA-type computational models.

When we examine the plot of atomic radius (or atomic volume) with respect to actinide element in Fig. 4(b),<sup>10</sup> we can see that the upturn that occurs just before Pu is coincident with the turning off of the delocalization perturbation to the intermediate coupling scheme. The shutting off of the delocalization perturbation to the intermediate coupling model would explain much of the underlying cause of the success of the recent sophisticated but sometimes unorthodox modeling of Pu electronic structure. These improved approaches include the *ad hoc* localization of the 5f states,<sup>39</sup> inclusion of magnetic polarization in both  $\delta$ -Pu (Refs. 21, 40, and 41) and  $\alpha$ -Pu,<sup>21,42</sup> a strongly relativistic, spin-orbit-split model,<sup>43</sup> and Kondo-type electron correlation.<sup>2</sup> It is also consistent with recent experimental work that reports localization effects in  $\delta$ -Pu.<sup>44</sup> Finally, the turning off of the delocalization perturbation to the intermediate coupling states occurs prior to the large volume change between  $\alpha$ -Pu and

$\alpha$ -Pu, suggesting that electronic changes are occurring well before the Pu volume anomaly.

Thus, our simple picture of the Pu  $5f$  electronic structure can be summarized in the illustration shown in Fig. 4(c). There exist two lobes to the  $5f$  density, one (nominally  $5f_{5/2}$ ) crossing the Fermi level and mainly occupied and the other (nominally  $5f_{7/2}$ ) above the Fermi level and essentially unoccupied. Of course, there is mixing between the upper and lower lobes, such that the “ $5f_{5/2}$ ” lobe has some  $5f_{7/2}$  character and the “ $5f_{7/2}$ ” lobe has some  $5f_{5/2}$  character. However, if the mixing perturbation is weak, then the lower lobe (“ $5f_{5/2}$ ”) will retain a maximum occupation number of approximately 6 and the upper lobe (“ $5f_{7/2}$ ”) will retain a maximum occupation number of approximately 8. For  $\alpha$ -Pu, we estimate that  $n=5$ , so the lower lobe (“ $5f_{5/2}$ ”) is almost completely filled, with only one hole above the Fermi level. The upper lobe (“ $5f_{7/2}$ ”) is essentially empty. The next question is the following: Is the above simple, spectroscopically derived model supported by any calculations of the  $5f$  density of states? The answer is yes, as will be discussed below.

However, it is first necessary to consider the issue of the nonmagnetic nature of Pu. Despite the report of Meot-Reymond and Fournier,<sup>45</sup> there is no hard experimental evidence for a permanent magnetic moment in Pu, consistent with earlier reports.<sup>46,47</sup> However, recent magnetic susceptibility<sup>45,48</sup> and specific heat measurements<sup>49</sup> do point toward an internal complexity in the electronic structure which might be due to spin and orbital polarization of the  $5f$  states, with a net cancellation on each and every Pu atom. To achieve such a cancellation, there are many possibilities, including the following: Kondo shielding,<sup>45,50</sup> noncollinearity of vectors,<sup>51</sup> spin fluctuations,<sup>52</sup> and averaging over nearly degenerate states,<sup>21</sup> which is in fact a mathematical approximation to the concept of spin fluctuations. It is the averaging over degenerate states and hence spin fluctuations which lies at the core of the goal of the calculations presented in Fig. 1, under the column entitled “Antiferromagnetic.” Thus, while a nominal AF alignment is utilized in the calculation, the model strives for a net zero moment on each individual Pu atom, approximating what may be a dynamical shielding with an averaging over several nearly degenerate but static states.

Thus consider what is observed in Fig. 1. The unit cell of  $\alpha$ -Pu has 16 atoms, with two each of eight different types.<sup>42</sup> Clearly, there are two well-defined lobes, with the Fermi level ( $E=0$  eV) crossing the lower lobe (“ $5f_{5/2}$ ”), in each panel for both the AF and nonmagnetic cases. The AF case has a lower energy minimization than the NM case, but both have roughly the same relative volume (see Fig. 2 in Ref. 21). In fact, the NM case does look slightly more like our simple model shown in Fig. 4(c).

As was already indicated in the work by Sadigh, Söderlind, and Wolfer,<sup>42</sup> the localized moments in  $\alpha$ -Pu are either dynamically screened in such a way as to not respond to applied magnetic fields, or the total magnetic moment is zero due to cancellation of spin and orbital contributions. In the present RSPFLAPW-based calculations there is some evidence for both of the above possibilities. First, two calcula-

tions with different orientations of the moments on atoms (both of them are AF type) have resulted in practically the same total energies. Quite possibly, there are other magnetic orderings (configurations) in  $\alpha$ -Pu with almost the same energies, and the true ground state of  $\alpha$ -Pu can be expressed as a linear combination of these configurations. DFT is a one-particle theory, and there can only be one of the configurations in the calculation. This circumstance may be a reason for some disagreements between calculated equilibrium properties of  $\alpha$ -Pu and experimental ones. Another effect of a possible mixing of magnetic configurations may consist in screening of the local magnetic moments, which have been obtained in AF calculations. If it is true, this effect explains the possible temperature independence of magnetic susceptibility in  $\alpha$ -Pu.<sup>45</sup> Second, in our calculations the spin magnetic moments are always directed opposite to the orbital magnetic moments on all of the atoms, though the cancellation is not complete in the calculations. In relation to this fact, it is interesting to consider the differential (with respect to energy) spin and orbital magnetic moments as shown in Fig. 5, in which the differential spin moments are dashed (green) and orbital moments solid (red). The meaning of these functions is that they, after being integrated to the Fermi energy, give correspondingly the local spin or orbital magnetic moments on the atom in question. The analysis of them and the corresponding magnetic moments, as shown in Table II for all of the eight different atoms in  $\alpha$ -Pu, tells us that a lowering of the Fermi level would result in a more complete cancellation between spin and orbital magnetic moments. The lowering of the Fermi level might be a result of more localized behavior for some states than is in our calculations. So, it is quite possible that the Fermi level is artificially too high in our calculations due some restrictions related to the GGA and in reality there may be a complete cancellation of spin and orbital magnetic moments.

Similar nonmagnetic calculations have been performed for  $\alpha$ -Th and  $\alpha$ -U, as shown in Fig. 6. These calculations include the identification of the  $5f^{5/2}$  and  $5f^{7/2}$  contributions. The two-lobe structure is clearly visible in the case of  $\alpha$ -Th and this is consistent with bremsstrahlung isochromat spectroscopy (BIS) result of Baer and Lang,<sup>24</sup> shown as an inset in Fig. 6. Because of the high energy (1487 eV) of the transition used in BIS, the BIS spectrum can provide a fairly accurate if somewhat broadened picture of the *unoccupied* density of states above the Fermi level. (Thus in comparing BIS to the DOS calculations here, one should only look at the calculated DOS above the Fermi level. In BIS, the spectral transitions are forbidden to states below the Fermi level, leading to a sharp drop-off or step at the Fermi level ( $E=0$  eV) in the BIS data. This can be misleading in the case of the U BIS. In U, the sharp Fermi edge cutoff at 0 eV causes the BIS spectrum to be truncated and makes it appear to be more “two lobed” than it actually is. Again, BIS measures only the unoccupied DOS, not anything below the Fermi level.) In the case of thorium, it is clear that only a limited amount of mixing of the  $5f^{5/2}$  and  $5f^{7/2}$  states is occurring. In the middle panel, the corresponding results are shown for  $\alpha$ -U. Again, there is a strong agreement between the calculated DOS and the BIS of U, if the “1 eV” broadening of the

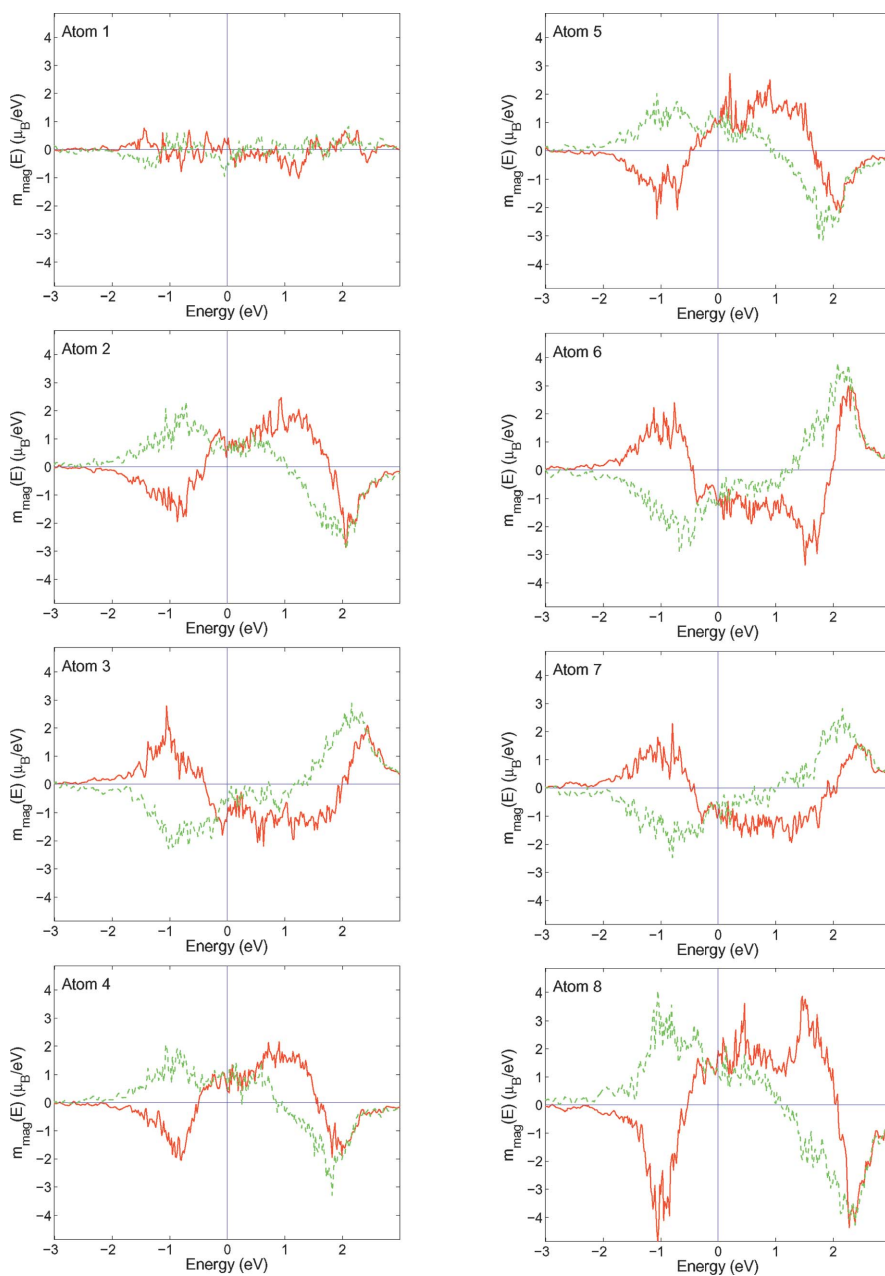


FIG. 5. (Color) Differential spin and orbital magnetic moments in  $\alpha$ -Pu, for each site type in the unit cell.

BIS measurements is taken into account, with peaks at 1/2 and 2 eV and a minimum near 1 eV, relative to the Fermi level at 0 eV. Here again, the impact of increased relative delocalization in U can be observed: instead of two strongly lobed features as in Th and Pu, the DOS of U is “smeared out,” above and below the Fermi level and there is a strong mixing and diminished separation of the  $5f^{5/2}$  and  $5f^{7/2}$  contributions.

Finally, in the lowermost panel of Fig. 6, the DOS of a representative atom from  $\alpha$ -Pu is shown, with a breakdown

into states composed of  $5f^{5/2}$  and  $5f^{7/2}$  origin. Clearly, the lower lobe is predominantly of  $5f^{5/2}$  character and the upper lobe is predominantly of  $5f^{7/2}$  character, but significant mixing is occurring, consistent with the intermediate coupling model used in the spectral analysis above and our illustration shown in Fig. 4(c). As can be seen in Table III, this trend is observed in all eight of the atomic sites in the  $\alpha$ -Pu unit cell. Thus it is obvious, even in  $\alpha$ -Pu, that the delocalization perturbation is a secondary effect relative to the spin-orbit splitting of the  $5f$  states.

TABLE II. Nominal spin and orbital magnetic moments on each site type within the  $\alpha$ -Pu unit cell.

Atom	1	2	3	4	5	6	7	8
$M_{\text{spin}}$	-0.46	2.22	-2.62	2.07	2.20	-2.80	-2.44	3.54
$M_{\text{orb}}$	0.18	-1.00	0.99	-0.94	-1.09	1.24	1.03	-1.65

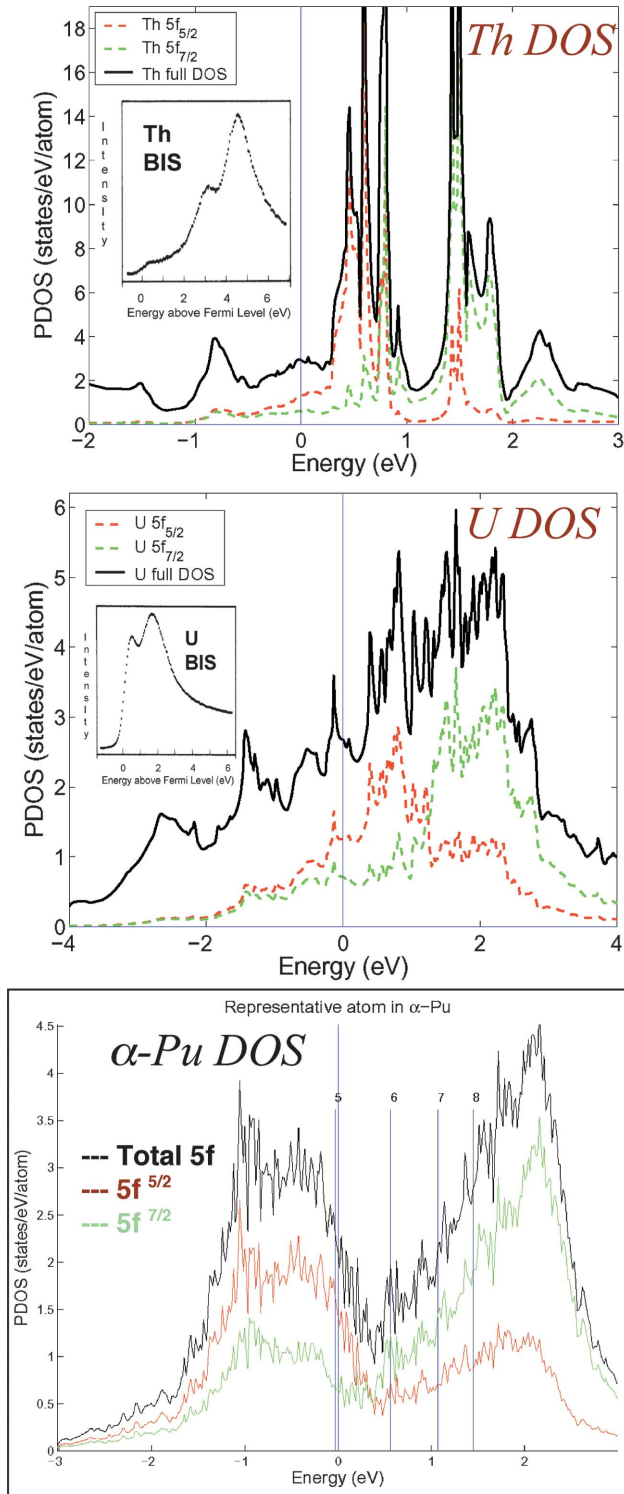


FIG. 6. (Color) DOS of  $\alpha$ -Th,  $\alpha$ -U, and  $\alpha$ -Pu, as described in the text. The Th and U BIS data, shown as insets, are from Baer and Lang (Ref. 24). The blue vertical lines with numerical annotations in the  $\alpha$ -Pu calculation correspond to various occupations ( $n$ ) of the Pu  $5f$  states. For Pu,  $n \approx 5$ .

#### IV. CONCLUSIONS

In itinerant metals, such as the  $3d$  series, the spin-orbit interaction is quenched by the band structure and the crystal

TABLE III. Percentage angular momentum character of the lower lobe (peak 1) and upper lobe (peak 2) in the density of states of  $\alpha$ -Pu.

Atom	Peak	$s$	$p$	$d$	$f(5/2)$	$f(7/2)$
1	1	1.3	1.6	14.9	53.1	29.0
	2	1.4	3.4	14.8	21.8	58.6
2	1	1.5	2.0	13.7	53.4	29.5
	2	1.1	3.1	16.1	21.9	57.7
3	1	1.5	2.0	14.2	51.4	30.9
	2	1.1	3.2	15.3	23.2	57.2
4	1	1.6	2.1	13.5	54.2	28.7
	2	1.0	3.2	15.9	21.3	58.5
5	1	1.5	2.1	13.7	53.7	29.0
	2	1.0	3.1	15.9	21.7	58.3
6	1	1.5	2.0	13.8	52.1	30.6
	2	1.1	3.1	16.1	22.7	57.0
7	1	1.4	2.0	14.1	51.3	31.2
	2	1.2	3.1	15.4	23.5	56.9
8	1	1.6	2.4	11.9	51.8	32.4
	2	0.8	2.7	17.9	23.2	55.3

field, which make its value small. On the other hand, in localized rare earth metals the  $4f$  spin-orbit interaction is not quenched, but will be close to the Hund's rule ground-state value. For the actinides, our results show that a picture with an intermediate coupling model skewed toward a  $jj$  limit, and with a delocalization perturbation, is appropriate, and that in using the sum rule we are able to quantify this. Because of its low occupation, the Th result is consistent with all three angular momentum coupling schemes:  $LS$ , intermediate coupling, and  $jj$ . The Pu results clearly point to the necessity of an intermediate scheme, with a strong  $jj$  inclination. The U results, while superficially pointing toward an  $LS$  picture, are in fact indicative of an intermediate coupling model with delocalization effects. The improved GGA LDA calculations support these conclusions drawn from the spectroscopic study and indicate that the spin-orbit splitting of the  $5f$  states is on the scale of 1.5–2 eV, as shown in Figs. 1 and 6. A key result here is that simplistic models that work well for U, e.g., simpler LDA-type models with delocalization and  $LS$  coupling, must fail for Pu. Between U and Pu, the delocalization perturbation effectively becomes almost negligible, although the broadening of the lobes observed in Figs. 1 and 6 suggest that remnant hybridization and delocalization are occurring. For Pu, modeling that diminishes delocalization effects will be most appropriate.<sup>21,39–43</sup> Finally and most importantly, while some level of delocalization and concomitant hybridization with the  $d$  states must be occurring in Pu,<sup>53</sup>  $5f$  delocalization is a secondary effect relative to the  $5f$  spin-orbit splitting for Pu.

#### ACKNOWLEDGMENTS

This work was performed under the auspices of the U.S. DOE by University of California Lawrence Livermore Na-

tional Laboratory under Contract No. W-7405-Eng-48. The ALS and the Spectromicroscopy Facility (Beamline 7.0) have been built and operated under funding from the Office of Basic Energy Science at DOE. The authors wish to thank

J. Lashley and M. Blau for synthesis of the Pu samples used at the ALS and D. Shuh, R. Schulze, J. Terry, J. D. Farr, T. Zocco, K. Heinzelman, and E. Rotenberg, for help with the data collection at the ALS.

\*Corresponding author. FAX: 925-423-7040. Email address: Tobin1@LLNL.Gov

- <sup>1</sup>R. C. Albers, *Nature* (London) **410**, 759 (2001).
- <sup>2</sup>S. Y. Savrasov, G. Kotliar, and E. Abrahams, *Nature* (London) **410**, 793 (2001).
- <sup>3</sup>G. Lander, *Science* **301**, 1057 (2003).
- <sup>4</sup>X. Dai S. Y. Savrasov, G. Kotliar, A. Migliori, H. Ledbetter, and E. Abrams, *Science* **300**, 953 (2003).
- <sup>5</sup>J. Wong M. Krisch, D. L. Farber, F. Occelli, A. J. Schwartz, T. C. Chiang, M. Wall, C. Boro, and R. Xu, *Science* **301**, 1078 (2003).
- <sup>6</sup>J. L. Sarrao, L. A. Morales, J. D. Thompson, B. L. Scott, G. R. Stewart, F. Wastin, J. Rebizant, P. Boulet, E. Colineau, and G. H. Lander, *Nature* (London) **420**, 297 (2002).
- <sup>7</sup>I. Opahle and P. M. Oppeneer, *Phys. Rev. Lett.* **90**, 157001 (2003).
- <sup>8</sup>T. Maehiro, T. Hotta, K. Ueda, and A. Hasegawa, *Phys. Rev. Lett.* **90**, 207007 (2003).
- <sup>9</sup>P. Soderlind, *Europhys. Lett.* **55**, 525 (2001).
- <sup>10</sup>S. S. Hecker, *MRS Bull.* **26**, 872 (2001), and reference therein.
- <sup>11</sup>G. van der Laan and B. T. Thole, *Phys. Rev. Lett.* **60**, 1977 (1988).
- <sup>12</sup>B. T. Thole and G. van der Laan, *Phys. Rev. B* **38**, 3158 (1988).
- <sup>13</sup>G. van der Laan and B. T. Thole, *Phys. Rev. B* **53**, 14 458 (1996).
- <sup>14</sup>R. Baptist, D. Courteix, J. Chayrouse, and L. Heintz, *J. Phys. F: Met. Phys.* **12**, 2103 (1982).
- <sup>15</sup>K. T. Moore, B. W. Chung, S. A. Morton, A. J. Schwarz, J. G. Tobin, S. Lazar, F. D. Tichelaar, H. W. Zandbergen, P. Soderlind, and G. van der Laan, *Phys. Rev. B* **69**, 193104 (2004), and references therein.
- <sup>16</sup>M. A. Wall, A. J. Schwartz, and M. J. Fluss, *Sample Preparation for Transmission Electron Microscopy Characterization of Pu Alloys*, Lawrence Livermore National Laboratory, Report No. UCRL-ID-141746.
- <sup>17</sup>K. T. Moore, M. A. Wall, and A. J. Schwartz, *J. Nucl. Mater.* **306**, 213 (2002).
- <sup>18</sup>J. G. Tobin B. W. Chung, R. K. Schulze, J. Terry, J. D. Farr, D. K. Shuh, K. Heinzelman, E. Rotenberg, G. D. Waddill, and G. Van der Laan, *Phys. Rev. B* **68**, 155109 (2003).
- <sup>19</sup>G. van der Laan, K. T. Moore, J. G. Tobin, B. W. Chung, M. A. Wall, and A. J. Schwartz, *Phys. Rev. Lett.* **93**, 097401 (2004).
- <sup>20</sup>J. P. Perdew, K. Burke, and M. Ernzerhof, *Phys. Rev. Lett.* **77**, 3865 (1996).
- <sup>21</sup>A. L. Kutepov and S. G. Kutepova, *J. Phys.: Condens. Matter* **15**, 2607 (2003); A. L. Kutepov, Lawrence Livermore National Laboratory Report No. UCRL-TR-200654.
- <sup>22</sup>G. Kalkowski, G. Kaindl, W. D. Brewer, and W. Krone, *Phys. Rev. B* **35**, 2667 (1987). The peak ratio of the  $N_{4,5}$  edge is given in the first complete paragraph on p. 2675.
- <sup>23</sup>B. T. Thole, G. van der Laan, J. C. Fuggle, G. A. Sawatzky, R. C. Karnatak, and J. M. Esteve, *Phys. Rev. B* **32**, 5107 (1985).
- <sup>24</sup>G. van der Laan, B. T. Thole, G. A. Sawatzky, J. C. Fuggle, and R. Karnatak, *J. Phys. C* **19**, 817 (1986).
- <sup>25</sup>K. T. Moore, M. A. Wall, A. J. Schwartz, B. W. Chung, D. K. Shuh, R. K. Schulze, and J. G. Tobin, *Phys. Rev. Lett.* **90**, 196404 (2003).
- <sup>26</sup>Y. Baer and J. K. Lang, *Phys. Rev. B* **21**, 2060 (1980).
- <sup>27</sup>J. R. Naegele, in *Actinides and some of their alloys and compounds*, in *Electronic Structure of Solids: Photoemission Spectra and Related Data*, edited by A. Goldmann, Landolt-Börnstein, Group III Vol. 23B, 183(1994).
- <sup>28</sup>R. G. Denning J. C. Green, T. E. Hutchings, C. Dallera, A. Tagliaferri, K. Giardi, N. B. Brookes, and L. Braichovich, *J. Chem. Phys.* **117**, 8008 (2002).
- <sup>29</sup>J. C. Kruppa, E. Simoni, J. Sytsma, and N. Edelstein, *J. Alloys Compd.* **213/214**, 471 (1994).
- <sup>30</sup>H. L. Skriver and J.-P. Jan, *Phys. Rev. B* **21**, 1489 (1980).
- <sup>31</sup>H. L. Skriver, O. K. Anderson, and B. Johansson, *Phys. Rev. Lett.* **41**, 42 (1978).
- <sup>32</sup>B. Johansson *et al.*, H. L. Skriver, N. Martensson, O. K. Andersen, and D. Gloetzel, *Physica B* **102B**, 12 (1980).
- <sup>33</sup>J. F. Herbst, R. E. Watson, and I. Lindgren, *Phys. Rev. B* **14**, 3265 (1976).
- <sup>34</sup>Y. Baer, *Physica B* **102**, 104 (1980).
- <sup>35</sup>A. Zangwill and D. A. Liberman, *Phys. Rev. B* **36**, 6705 (1987).
- <sup>36</sup>C. Laubschat, W. Grentz, and G. Kaindl, *Phys. Rev. B* **37**, 8082 (1988).
- <sup>37</sup>B. T. Thole and G. van der Laan, *Phys. Rev. A* **38**, 1943 (1988).
- <sup>38</sup>P. Soderlind, *Adv. Phys.* **47**, 959 (1998).
- <sup>39</sup>J. M. Wills, O. Eriksson, A. Delin, P. H. Andersson, J. J. Joyce, T. Durakiewicz, M. T. Butterfield, A. J. Arko, D. P. Moore, and L. A. Morales, *J. Electron Spectrosc. Relat. Phenom.* **135**, 163 (2004); J. J. Joyce *et al.*, *Phys. Rev. Lett.* **91**, 176401 (2003).
- <sup>40</sup>S. Y. Savrasov and G. Kotliar, *Phys. Rev. Lett.* **84**, 3670 (2000).
- <sup>41</sup>P. Soderlind, A. L. Landa, and B. Sadigh, *Phys. Rev. B* **66**, 205109 (2002); P. Soderlind and B. Sadigh, *Phys. Rev. Lett.* **92**, 185702 (2004).
- <sup>42</sup>B. Sadigh, P. Soderlind, and W. G. Wolfer, *Phys. Rev. B* **68**, 241101(R) (2003).
- <sup>43</sup>M. Penicaud, *J. Phys.: Condens. Matter* **9**, 6341 (1997).
- <sup>44</sup>L. Havela, T. Gouder, F. Wastin, and J. Rebizant, *Phys. Rev. B* **65**, 235118 (2003).
- <sup>45</sup>S. Meot-Reymond and J. M. Fourier, *J. Alloys Compd.* **232**, 119 (1996).
- <sup>46</sup>J. C. Lashley, A. W. Lawson, R. B. McQueeney, and G. H. Lander, *Phys. Rev. B* (to be published); Los Alamos National Laboratory Report No. LA-UR-04-3439, and references therein.
- <sup>47</sup>W. Nellis (private communication).
- <sup>48</sup>M. Fluss, private communication.
- <sup>49</sup>J. C. Lashley, J. Singleton, A. Migliori, J. B. Betts, R. A. Fisher, J. L. Smith, and R. J. McQueeney, *Phys. Rev. Lett.* **91**, 205901 (2003).
- <sup>50</sup>G. Kotliar and D. Volhardt, *Phys. Today* **57**, 53 (2004).

<sup>51</sup>Michael Brooks (private communication).

<sup>52</sup>A. J. Arko, M. B. Brodsky, and W. J. Nellis, *Phys. Rev. B* **5**, 4564 (1972).

<sup>53</sup>B. Cooper A. Banerjea, N. Kioussis, and J. M.Wills, *J. Less-*

*Common Met.* **121**, 271 (1986) and references therein;B. R. Cooper, *Handbook of the Physics and Chemistry of the Actinides*, edited by A. J. Freeman and G. H. Lander (Elsevier Science, Amsterdam, 1985), Vol. 2, page 435 (1985).